Supplemental Material for:

Controllable Design 3D Hierarchical Co/Ni-POM Nanoflower Compounds Supported on Ni foam for Hydrogen Evolution Reaction

Zhuanfang Zhang[a*], Yuanyuan Meng[b], Haolun Su[b], GuoHua Dong[b], Bing Zhao[b], Wenzhi Zhang[b], Guangming Yin[a], Yongzhi Liu[a]

[a]Center of Teaching Experiment Management Equiment, Qiqihar University, Qiqihar 161006, China

[b]College of Chemistry and Chemical Engineering, Heilongjiang Provincial Key Laboratory of Surface Active Agent and Auxiliary，Qiqihar University, Qiqihar 161006, P. R. China.

*Corresponding author. E-mail: zzfhao2014@163.com,

Contents

Section I Experimental

Synthesis of the Co/Ni-POM/NF

The Co/Ni-POM/NF material was prepared by using a modified hydrothermal method. Firstly, a 1×2 cm^2 block of commercial Ni foam was washed by using acetone, aqueous HCl solution (2.0 M), deionized water and ethanol in turn, then, dried at room temperature.

Secondly, 0.18 g $Co(NO_3)_2\cdot 6H_2O$ and 0.32 g $H_3[PMo_{12}O_{40}]\cdot 6H_2O$ were dissolved in 40 mL a mixture of water and alcohol(V_{Water}:$V_{alcohol}$). The solution was ultrasonic treated at room temperature for 30 minutes, and then it was transferred to 50 mL Teflon-lined autoclave. Then the treated Ni foam was immersed in above solution. After heating at 180℃ for 6h and naturally cooling. The generated material (named Co/Ni-POM-6h/NF) was washed with water three times and dried at 60℃ for 24 h. For comparison, Co/NF and POM/NF were prepared. The processes used for the synthesis of Co/NF and POM/NF are equal to synthesis of Co/Ni-POM/NF, except that there is only one type of ($Co(NO_3)_2\cdot 6H_2O$ or $H_3[PMo_{12}O_{40}]\cdot 6H_2O$).

In addition, in order to understand the relationship between morphology and performance, a series of comparative experiments were carried out. The other composites were obtained by changing reaction times, reaction temperature and reaction solvent. Table S1 lists the rules for naming samples.

Electrochemical measurements

All electrochemical tests were performed in a three-electrode system on the CHI700E work station. Graphite rod was used counter electrode, Hg/HgO was used the reference electrode, respectively. Samples were used as the working electrode with surface area of 1×2 cm^2. All Linear sweep voltammogram (LSV) curves were measured at the scan rate of 5mV·s^{-1} in 1M KOH buffer solution and without iR based correction. The potentials were calibrated with reference to reversible hydrogen electrode (RHE). RHE calibration according to the Nernst equation: $E_{RHE} = E_{Hg/HgO} + 0.059pH + 0.1084$. The Tafel equation ($\eta = b\log j + a$, where η is the overpotential, j is the current density and b is the Tafel slope. The values of exchange current density (j_0) are calculated according to extrapolating the Tafel slopes. Electrochemical impedance spectroscopy (EIS) data of the samples were collected over the frequency range 0.01–10^5 Hz. The double layer capacitances were obtained through cyclic voltammograms (CV), in which CV test was conducted with different scan rates from 20 to 100 mV s^{-1} in the potential range of -1.06–(-0.96) (vs. RHE). The durability test was carried out at a static overpotential for 34 h, during which the current variation with time was recorded.

Section II Supplementary Physical Characterizations

The purpose of title sample characterization is to study physical and chemical properties. The Fourier transform infraredspectroscopy (FT-IR) spectra were recorded by using a NICOLETiS10. The images of Scanning electron microscope (SEM) were obtained by using S4800 (Hitachi，acceleration voltage of 20 kV). The TEM and HR-TEM micrographs were obtained using Tecnai G2 F30 S-TWIN (FEI, operating at 300 kV).The X-ray powder diffraction (XRD) were obtained using Bruker-AXS (D8, Germany, Cu-Kα radiation, λ=1.5406 Å). X-Ray photoelectron spectroscopies (XPS) of patterns were performed by a VGESCALAB MK II (Mg-Kα, 1253.6 eV). The metallic elements were analyzed by using the inductively coupled plasma mass spectrometer (ICP-MS) (NexION 350X). The N_2 adsorption-desorption isotherms of the samples were performed by Autosorb-IQ3. All electrochemical measurements were tested using a CHI700E electrochemistry station.

1. **Fig. S1.** SEM image of bare nickel foam
2. **Fig.S2.** SEM images of (a) Co/Ni-POM-1h/NF, (b) Co/Ni-POM-3h/NF, (c) Co/Ni-POM-8h/NF, (d) Co/Ni-POM-10h/NF.
3. **Fig.S3**. XRD patterns of Co/Ni-POM-1h/NF、Co/Ni-POM-3h/NF、Co/Ni-POM-8h/NF and Co/Ni-POM-10h/NF.
4. **Fig.S4**. (a)Polarization curves， and (b) Tafel plotsof the catalysts with different hydrothermal time (Co/Ni-POM-1h/NF, Co/Ni-POM-3h/NF, Co/Ni-POM-8h/NF, Co/Ni-POM-10h/NF) in 1.0 M KOH.
5. **Fig. S5** The CVs of the catalysts recorded from -1.06 to -0.96 V at different rates from 20 to 100 mV s^{-1} for (a) Co/Ni-POM-1h/NF, (b) Co/Ni-POM-3h/NF, (c) Co/Ni-POM-8h/NF, (d) Co/Ni-POM-10h/NF.
6. **Fig.S6.** SEM images of the Co/Ni-POM in situ grown on the Ni foam using different reaction solvent. (a) V_{H2O}=40mL; (b) V_{Water}:$V_{alcohol}$ =2:1；(c) V_{Water}:$V_{alcohol}$=1:2; (d) $V_{alcohol}$=40mL.
7. **Fig.S7.** XRD patterns of Co/Ni-POM-1/NF、Co/Ni-POM-2/NF、Co/Ni-POM-3/NF and Co/Ni-POM-4/NF.
8. **Fig.S8.** (a)Polarization curves; and (b)Tafel plots of the catalysts with different solvent (Co/Ni-POM-1/NF, Co/Ni-POM-2/NF, Co/Ni-POM-3/NF, Co/Ni-POM-4/NF) in 1.0 M KOH.
9. **Fig. S9** The CVs of the catalysts recorded from -1.06 to -0.96 V at different rates from 20 to 100 mV s^{-1} for (a)Co/Ni-POM-1/NF, (b)Co/Ni-POM-2/NF, (c)Co/Ni-POM-3/NF, (d)Co/Ni-POM-4/NF) in 1.0 M KOH.
10. **Fig.S10.** SEM images of the Co/Ni-POM in situ grown on the Ni foam using different reaction temperature. (a) 110 °C;(b) 120 °C；c) 150 °C; (d) 200 °C.
11. **Fig.S11** XRD patterns of Co/Ni-POM-a/NF、Co/Ni-POM-b/NF、Co/Ni-POM-

c/NF and Co/Ni-POM-d/NF(time=6h, V_{Water}:$V_{alcohol}$ =1:1)

12. **Fig. S12.** (a)Polarization curves; and (b) Tafel plots for the catalysts with different solvent (Co/Ni-POM-a/NF, Co/Ni-POM-b/NF, Co/Ni-POM-c/NF, Co/Ni-POM-d/NF) in 1.0 M KOH.
13. **Fig. S13** The CVs of the catalysts recorded from -1.06 to -0.96 V at different rates from 20 to 100 mV s^{-1} for (a)Co/Ni-POM-a/NF, (b)Co/Ni-POM-b/NF, (c)Co/Ni-POM-c/NF, (d)Co/Ni-POM-d/NF) in 1.0 M KOH.
14. **Fig. S14.** (a) SEM image of Co/NF, (b) SEM image of POM/NF.
15. **Fig. S15.** Elemental mapping through SEM. (a-d) Elements mapping (Ni, O, Co, Mo) microsphere ;(e) EDX spectrum of Co/Ni-POM/NF.
16. **Fig. S16** Elemental mapping through SEM. (a-d) Elements mapping (Ni, O, Co, Mo) microsphere; (e) EDX spectrum of Co/Ni-POM power
17. **Fig. S17** N_2 sorption isotherms of NF, POMs/NF，Co/NF and Co/Ni-POMs-6h/NF
18. **Fig. S18.**The different scale SEM images of Co/Ni-POM fixed on Ni foam through adhesive
19. **Fig.S19**. Calculation of exchange current density of NF, Co/NF, POM/NF, Co/Ni-POM-6h/NF and Pt/C in 1.0 M KOH.
20. **Fig. S20**. (a)Polarization curves; (b) Tafel plots for Co/Ni-POM-6h/NF and Co/Ni-POM.
21. **Fig. S21** The Bode plot of NF, Co/NF, POM/NF, Co/Ni-POM-6h/NF at the entire frequency range.
22. **Fig. S22.** The CVs of the catalysts recorded from -1.06 to -0.96 V at different rates from 20 to 100 mV s^{-1} for (a) Co/NF; (b) POM/NF; and (c) Co/Ni-POM-6h/NF in 1.0 M KOH.
23. **Fig. S23**. CVs of (a) Co/NF, (b) POM/NF, and (c) Co/Ni-POM-6h/NF in 1 M PBS (pH = 6.89) with a scan rate of 50 mVs^{-1}. (d) Calculated TOF for Co/NF, POM/NF, Co/Ni-POM-6h/NF in 1 M KOH.
24. **Table S1.** The samples and their corresponding synthesis parameters.
25. **Table S2.** The comparison of the HER performance for Co/Ni-POM/NF at

different reaction condition in 1.0 M KOH.

26. **Table S3**. Comparison of HER activity of different POM-based composite catalysts.

Table S1. The samples and their corresponding synthesis parameters.

Entry	**Starting materials**	**The volume ratio of water/ alcohol**	**Hydrothermal Time (h)**	**reaction temperature (℃)**	**Final samples**
1	Co^{2+}/NF	1:1	6	180	Co/NF
2	POM/NF	1:1	6	180	POM/NF
3	Co^{2+}/POM/NF	1:1	1	180	Co/Ni-POM-1h/NF
4	Co^{2+}/POM/NF	1:1	3	180	Co/Ni-POM-3h/NF
5	Co^{2+}/POM/NF	1:1	6	180	Co/Ni-POM-6h/NF
6	Co^{2+}/POM/NF	1:1	8	180	Co/Ni-POM-8h/NF
7	Co^{2+}/POM/NF	1:1	10	180	Co/Ni-POM-10h/NF
8	Co^{2+}/POM/NF	V_{H2O}=40mL	6	180	Co/Ni-POM-1/NF
9	Co^{2+}/POM/NF	1:2	6	180	Co/Ni-POM-2/NF
10	Co^{2+}/POM/NF	2:1	6	180	Co/Ni-POM-3/NF
11	Co^{2+}/POM/NF	$V_{alcohol}$=40mL	6	180	Co/Ni-POM-4/NF
12	Co^{2+}/POM/NF	1:1	6	110	Co/Ni-POM-a/NF
13	Co^{2+}/POM/NF	1:1	6	120	Co/Ni-POM-b/NF
14	Co^{2+}/POM/NF	1:1	6	150	Co/Ni-POM-c/NF
15	Co^{2+}/POM/NF	1:1	6	200	Co/Ni-POM-d/NF

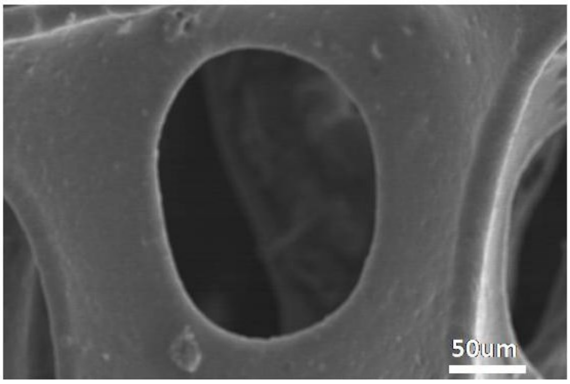

Fig. S1. SEM image of bare nickel foam

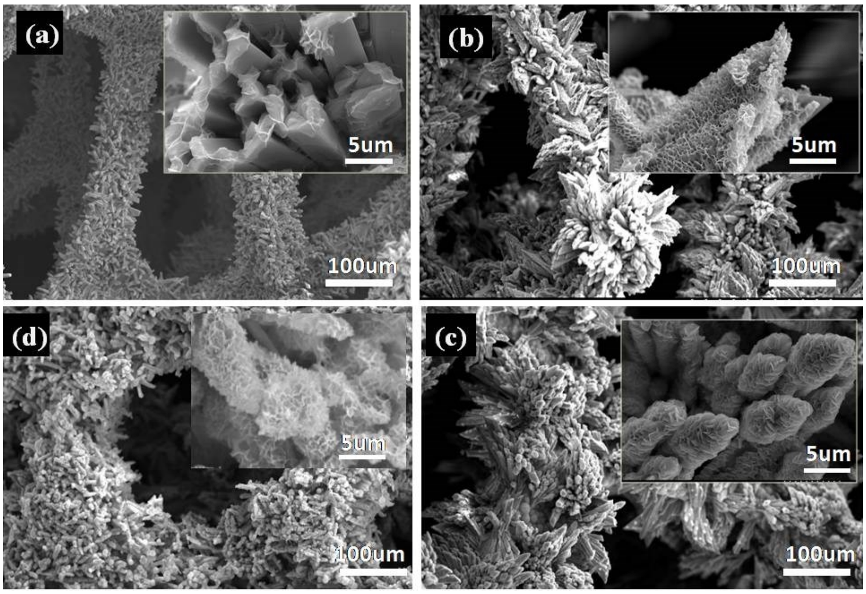

Fig.S2. SEM images of (a) Co/Ni-POM-1h/NF, (b) Co/Ni-POM-3h/NF, (c) Co/Ni-POM-8h/NF, (d) Co/Ni-POM-10h/NF.

In order to further understand the growth process of the Co/Ni-POM with three-dimensional nanoflowers in situ grown on Ni foam, a series of time-dependent experiments were carried out. The Co/Ni-POM/NF sample was hydrothermal treated at 180 ^{o}C for 1h, 3 h, 8 h and 10 h except 6 h, the panoramic SEM image (Fig. S2a-d) revealed that the different morphology of Co/Ni-POM onto the Ni foam under different reaction time. When the reaction time is 1h, the Co/Ni-POM distributed onto the Ni foam with columnar morphology, and there is little flake morphology structures on the pillar , as show in Fig. 2Sa.When the reaction time increase to 3 h, the more flake grows on cylindrical morphology (Fig. S2b). But with reaction increasing to 8 h, The Co/Ni-POM with ordered leaf-like structure covering on foamed nickel. Further prolonging the hydrothermal time to 10 h, the Co/Ni-POM /NF with disordered ball-like distributed onto the Ni foam, as show in Fig. S2d. The SEM tests demonstrate the formation of 3D nanoflowers of Co/Ni-POM /NF only in certain condition.

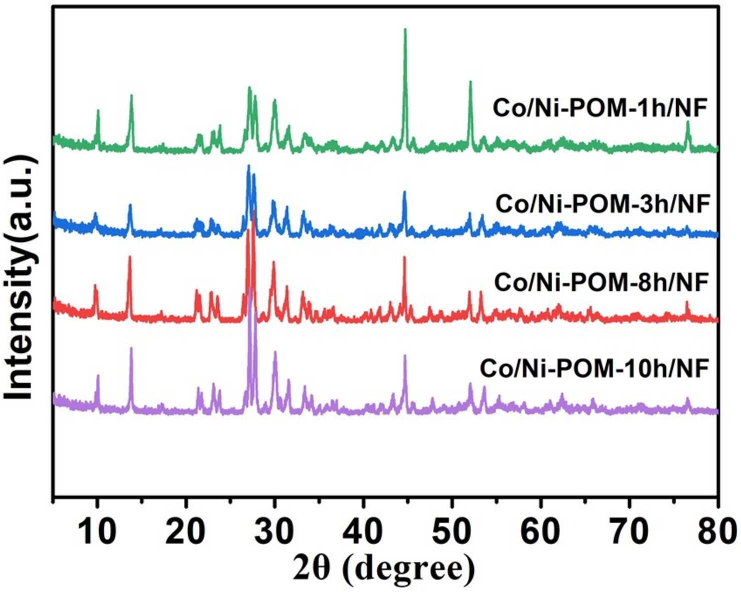

Fig.S3. XRD patterns of Co/Ni-POM-1h/NF, Co/Ni-POM-3h/NF, Co/Ni-POM-8h/NF and Co/Ni-POM-10h/NF.)

The samples from different calcination time are labeled as Co/Ni-POM-1h/NF、Co/Ni-POM-3h/NF、Co/Ni-POM-8h/NF and Co/Ni-POM-10h/NF, Fig. S3.The peak position have not changed at different calcination time, indicating that corresponding generated substances are basically the same.The XRD patterns indicate that the peak intensity of Co/Ni-POM increases with the increasing of calcination time.

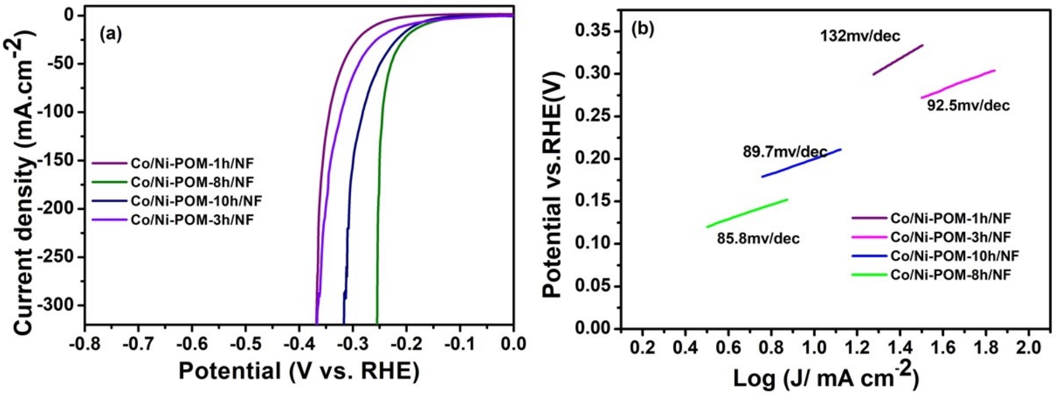

Fig.S4. Polarization curves and Tafel plots of the catalysts with different hydrothermal time (Co/Ni-POM-1h/NF, Co/Ni-POM-3h/NF, Co/Ni-POM-8h/NF, Co/Ni-POM-10h/NF) in (a, b) in 1.0 M KOH.

In order to study the morphology of Co/ Ni-POM for effect on performance，the electrocatalytic properties of control samples at different time were tested and compared，as show in Fig. S4. The catalyst for the hydrothermal treatment at short time (1h) had relatively poor HER activity, which was due to simple morphology at the initial stage. With the increase of the hydrothermal time, the HER activity gradually increases. The performance is best when the time is 6h，(tableS2). While for the sample from the longer hydrothermal time (8~10h), the HER activity falls because of the irregular and disordered state of morphology.

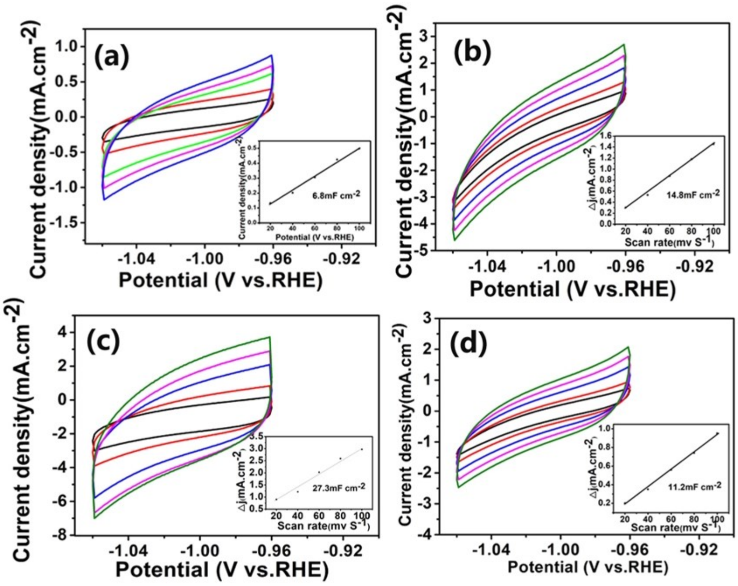

Fig. S5 The CVs of the catalysts recorded from -1.06 to -0.96 V at different rates from 20 to 100 mV s^{-1} for (a) Co/Ni-POM-1h/NF, (b) Co/Ni-POM-3h/NF, (c) Co/Ni-POM-8h/NF, (d) Co/Ni-POM-10h/NF.

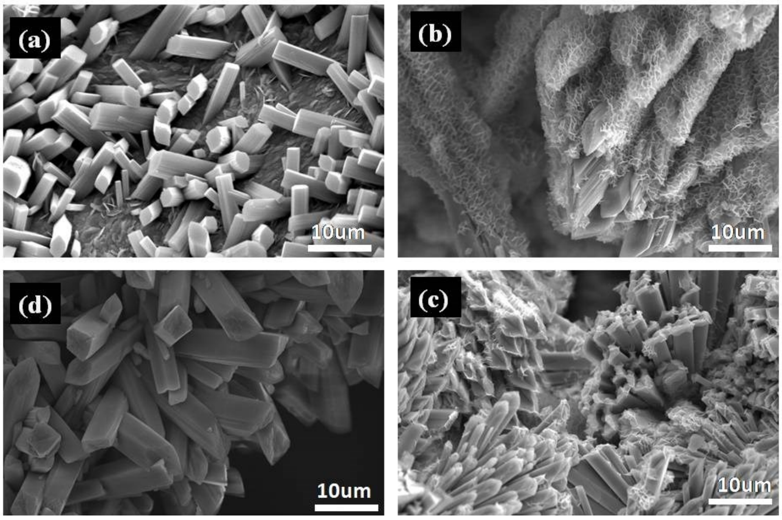

Fig.S6. SEM images of the Co/Ni-POM in situ grown on the Ni foam by using different reaction solvent. (a) V_{H2O}=40mL; (b) V_{Water}:$V_{alcohol}$ =2:1; (c) V_{Water}:$V_{alcohol}$=1:2; (d) $V_{alcohol}$=40mL (time=6h, temperature=180 °C)

In addition, the effect of different solvents for morphology of the Co/Ni-POM in situ grown on Ni foam was also studied. A series of the volume ratio of water to ethanol was compared. The panoramic SEM image (Fig. S6 a-d) revealed that the different morphology of Co/Ni-POM onto the Ni foam under different reaction solvent. When the solvent is all water, the Co/Ni-POM distributed onto the Ni foam with cylindrical morphology, which is disorganized and sparse as show in Fig.6 a. When the water and alcohol of volume ratio in the solvent changes to 2: 1, there are some flakes grows on cylindrical morphology, and the Co/Ni-POM of amount on foamed nickel has increased (Fig. S6b). But with reaction solvent is all alcohol, The Co/Ni-POM with ordered cylindrical structure covering on foamed nickel, without any flake on the pillars, Fig. S6d. The SEM tests demonstrate that the morphology of Co/Ni-POM was affected by the reaction solvent.

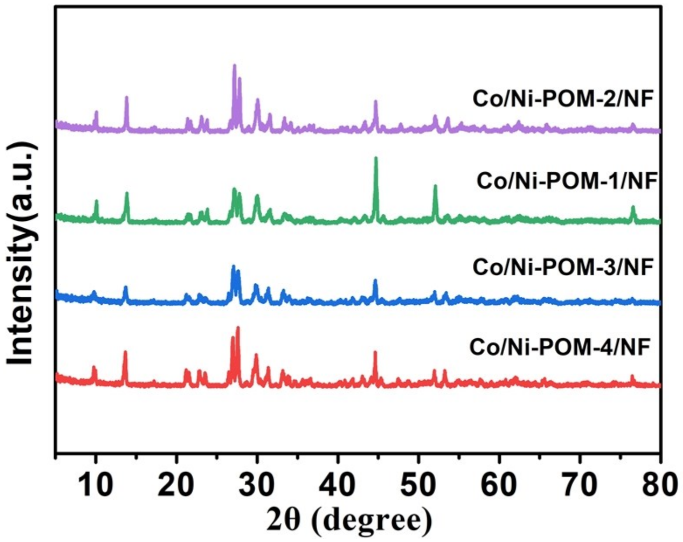

Fig.S7. XRD patterns of Co/Ni-POM-1/NF、Co/Ni-POM-2/NF、Co/Ni-POM-3/NF and Co/Ni-POM-4/NF.

The samples from different solvents are labeled as Co/Ni-POM-1/NF、Co/Ni-POM-3/NF、Co/Ni-POM-3/NF and Co/Ni-POM-4/NF. The peak position have not changed at different Solvent ratio, indicating that corresponding generated substances are basically the same. (Fig.S7).

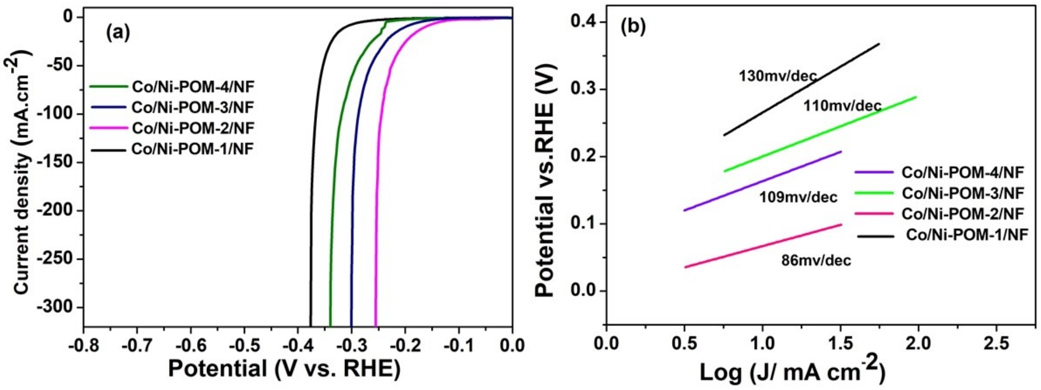

Fig. S8. (a) Polarization curves; (b)Tafel plots for the catalysts with different solvent (Co/Ni-POM-1/NF, Co/Ni-POM-2/NF, Co/Ni-POM-3/NF, Co/Ni-POM-4/NF) in 1.0 M KOH.

The catalyst for the hydrothermal different solvent has different catalytic activities. The Co/Ni-POM-1/NF had relatively poor HER activity, which was due to simple morphology with disorganized and sparse. The performance of Co/Ni-POM-2/NF is best among of four, because of the hierarchical of morphology (**Fig. S8**).

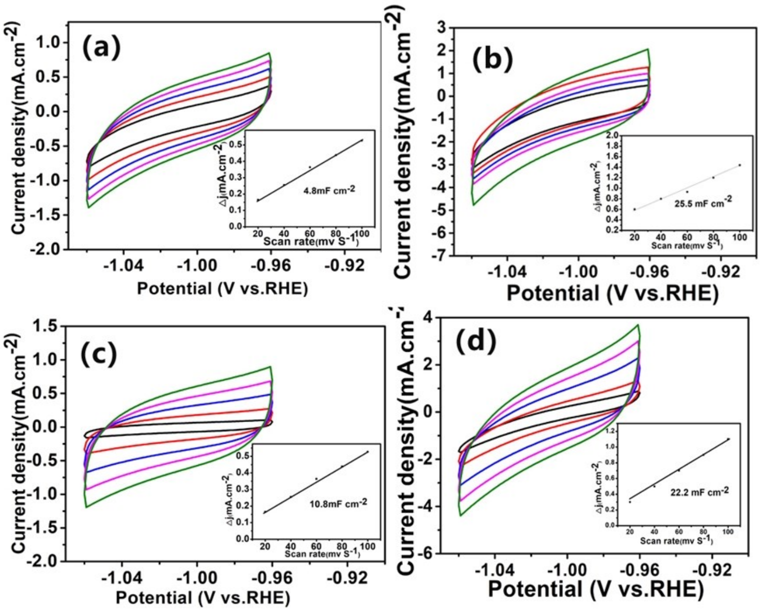

Fig. S9 The CVs of the catalysts recorded from -1.06 to -0.96 V at different rates from 20 to 100 mV s^{-1} for (a)Co/Ni-POM-1/NF, (b)Co/Ni-POM-2/NF, (c)Co/Ni-POM-3/NF, (d)Co/Ni-POM-4/NF) in 1.0 M KOH.

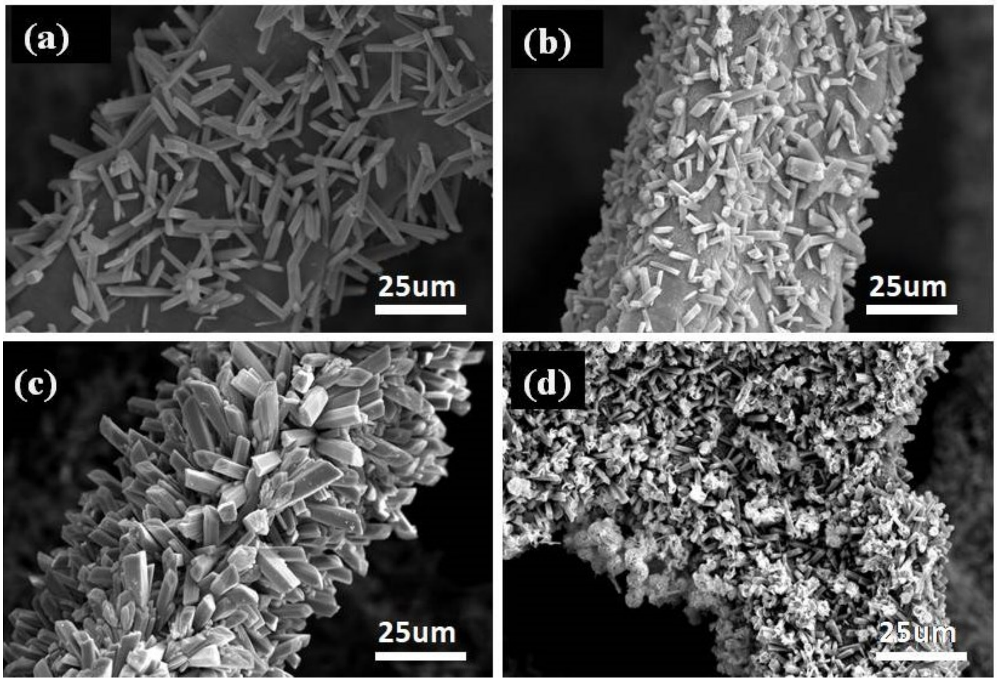

Fig.S10. SEM images of the Co/Ni-POM in situ grown on the Ni foam using different reaction temperature. (a) 110 °C;(b) 120 °C；(c) 150 °C; (d)200 °C.

It is also very important that the effect of reaction temperature on morphology. The SEM images of the Co/Ni-POM in situ grown on the Ni foam using different reaction temperature were further illustrated. When the reaction temperature is 110 °C, the Co/Ni-POM distributed onto the Ni foam with cylindrical morphology, which is disorganized and sparse as show in Fig. S10a. When reaction temperature is 120 °C, Co/Ni-POM is still sparsely distributed on the the Ni foam Fig. S10b. When reaction temperature is 150 °C, the morphology of Ni/Co-POM/NF was similar to that of Co/Ni-POM-6h /NF, in which the producted substance were uniform distributed on the the Ni foam, Fig. S10c. With reaction temperature rising to 200 °C, the hierarchical nanoflower structure was destroyed, and the Ni/Co-POM with cylindrical structure was densely distributed on foamed nickel, Fig. S10d.

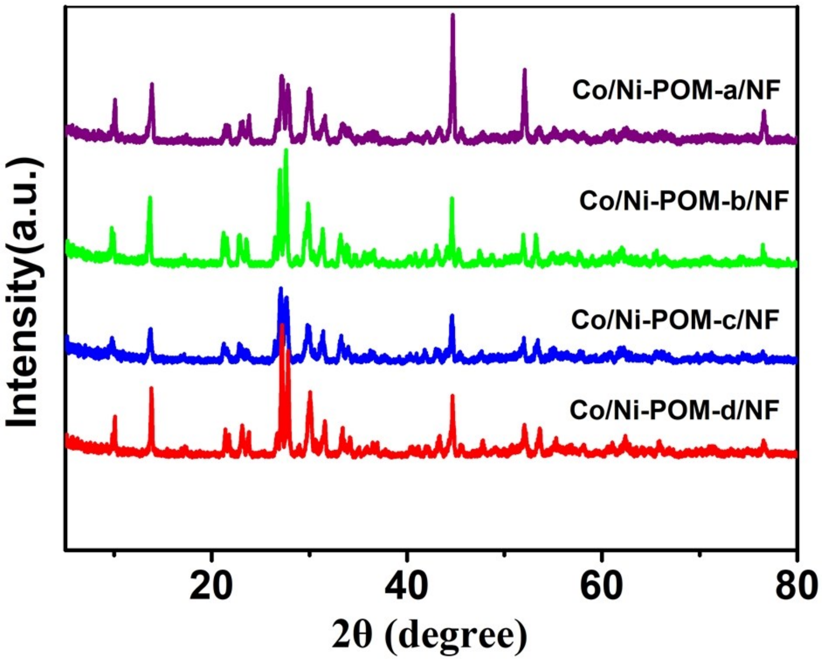

Fig.S11. XRD patterns of Co/Ni-POM-a/NF、Co/Ni-POM-b/NF、Co/Ni-POM-c/NF and Co/Ni-POM-d/NF.

The samples from different reaction temperature are labeled as Co/Ni-POM-a/NF、Co/Ni-POM-b/NF、Co/Ni-POM-c/NF and Co/Ni-POM-d/NF. The peak position have not changed at different Solvent ratio. Notably, because of same ingredients, the XRD patterns indicate that the composition and structure of all the samples are similar, (Fig.S11).

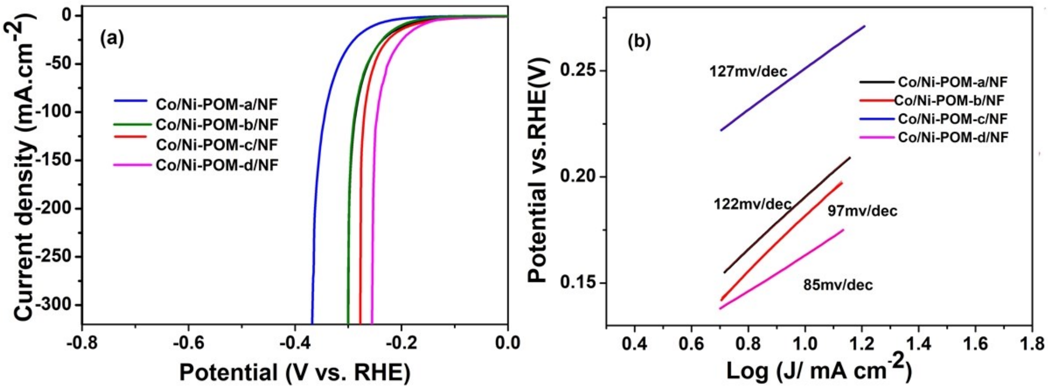

Fig. S12. (a)Polarization curves; (b) Tafel plots for the catalysts with different reaction temperature (Co/Ni-POM-a/NF, Co/Ni-POM-b/NF, Co/Ni-POM-c/NF, Co/Ni-POM-d/NF) in 1.0 M KOH.

The catalyst for different reaction temperature has different catalytic activities. The Co/Ni-POM-a/NF had relatively poor HER activity, which was due to simple morphology with disorganized and sparse. The HER performance of Co/Ni-POM-d/NF is best among of four, which is due to dense active material Co/Ni-POM in situ grown on the Ni foam (Fig. S12).

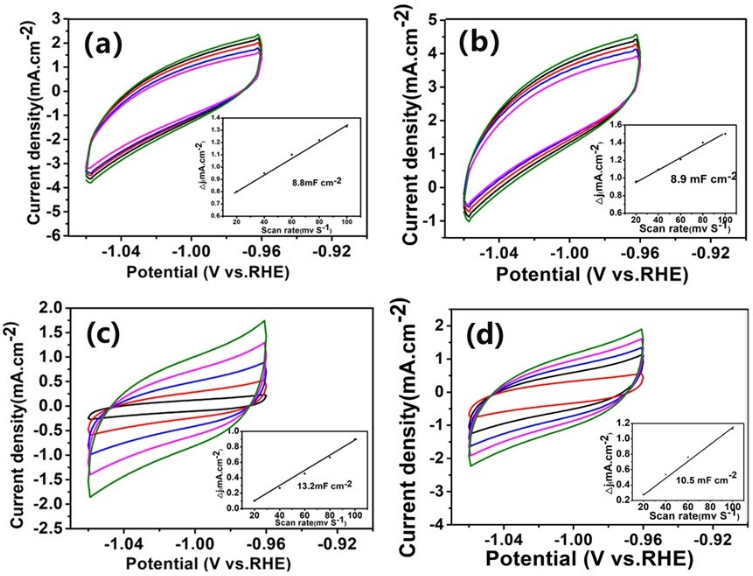

Fig. S13 The CVs of the catalysts recorded from -1.06 to -0.96 V at different rates from 20 to 100 mV s^{-1} for (a) Co/Ni-POM-a/NF, (b) Co/Ni-POM-b/NF, (c) Co/Ni-POM-c/NF, (d) Co/Ni-POM-d/NF) in 1.0 M KOH.

To evaluate the performance of electrocatalysts fairly, the kinetic parameters such as overpotential (η), Tafel slope and C_{dl} are required to be measured or calculated carefully, shown in table S2.

Table S2. The comparison of the HER performance for Co/Ni-POM/NF at different reaction condition in 1.0 M KOH.

Catalysts	**η_{10}, η_{100}, η_{200}(mV)**	**Tafel slopes (mV dec^{-1})**	C_{dl} (mF cm^{-2})
NF	324,453,473	136	-
Co/NF	218,379,400	97	25.3
POM/NF	288,325,349	125	9.8
Co/Ni-POM-1h/NF	255,341,360	132	6.8
Co/Ni-POM-3h/NF	203,314,349	92.5	14.8
Co/Ni-POM-6h/NF	68,123,132	60.8	61.2
Co/Ni-POM-8h/NF	163,239,349	85	27.3
Co/Ni-POM-10h/NF	177,279,305	89	11.2
Co/Ni-POM-1/NF	312,366,372	130	4.8
Co/Ni-POM-2/NF	157,242,251	86	25.5

Co/Ni-POM-3/NF	197,288,297	109	10.8
Co/Ni-POM-4/NF	240,318,331	110	22.2
Co/Ni-POM-a/NF	252,341,362	129	8.8
Co/Ni-POM-b/NF	201,282,296,	122	8.9
Co/Ni-POM-c/NF	172,263,274	97	13.2
Co/Ni-POM-d/NF	161,242,250	85	10.5

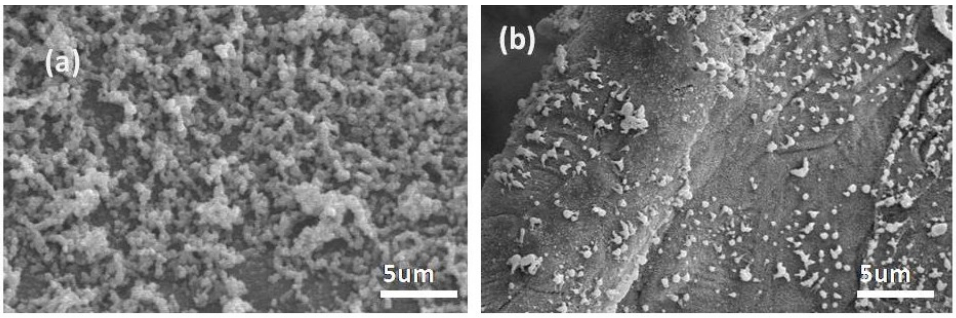

Fig. S14. SEM image of (a) Co/NF, and (b) POM/NF.

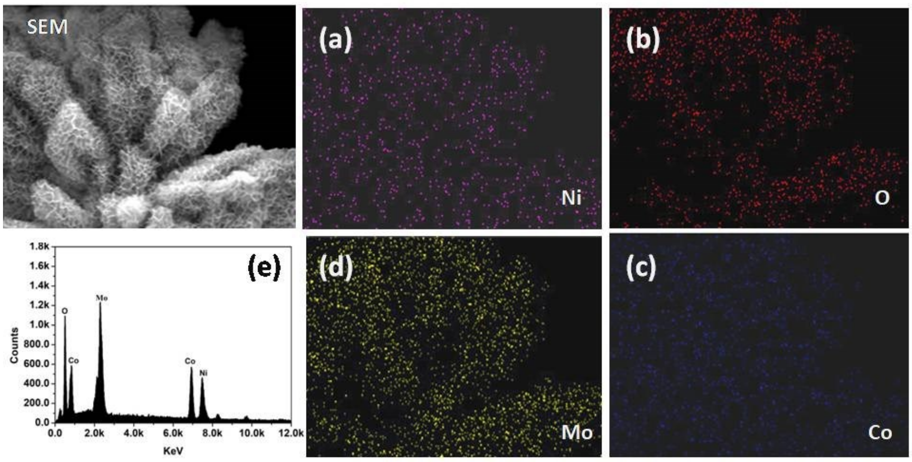

Fig. S15 Elemental mapping through SEM. (a-d) Elements mapping (Ni, O, Co, Mo) microsphere; (e) EDX spectrum of Co/Ni-POM/NF.

In this work, 0.18 g $Co(NO_3)_2{\cdot}6H_2O$ and 0.32 g $H_3[PMo_{12}O_{40}]{\cdot}6H_2O$ were dissolved in 40 mL a mixture of water and alcohol(V_{Water}:$V_{alcohol}$). The solution was ultrasonic treated at room temperature for 30 minutes, and then it was transferred to 50 mL Teflon-lined autoclave. Then the treated Ni foam was immersed in above solution. After heating at 180°C for 6h and naturally cooling. During the whole process of the hydrothermal reaction, some of the Co/Ni-POM composites grow in situ on the nickel foam, and some others grow spontaneously in the solution. The resulting suspension was filtered and washed with water three times and dried at 60 °C for 24 h to obtain the The Co/Ni-POM power. The EDX of the synthesized powder sample shows that the substance contained nickel element, as shown in **Fig. S16.**

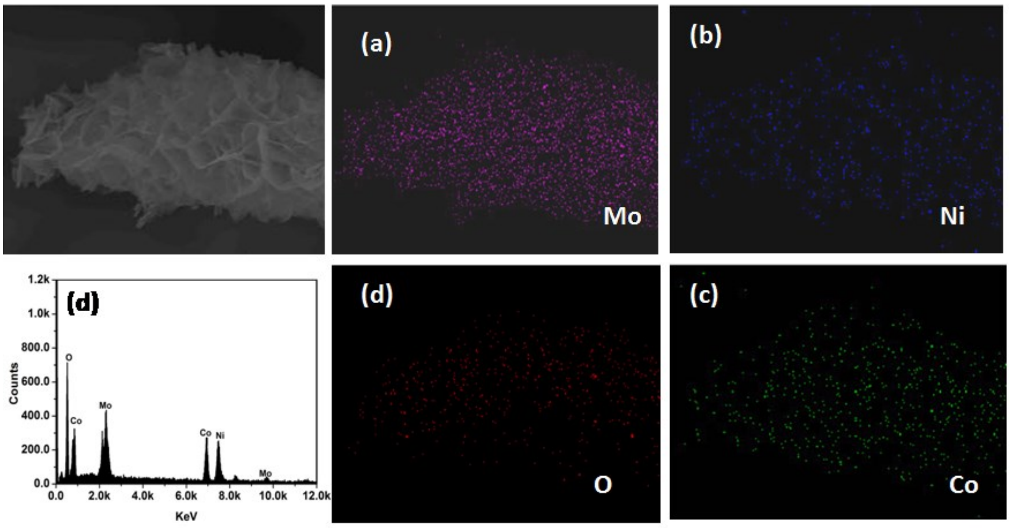

Fig. S16 Elemental mapping through SEM. (a-d) Elements mapping (Ni, O, Co, Mo) microsphere; (e) EDX spectrum of Co/Ni-POM power

The specific surface area of NF, POMs/NF，Co/NF and Co/POMs-6h/NF were determined by Autosorb-IQ3 II and calculated by Brunauer-EmmettTeller (BET) method. The N_2 adsorption-desorption isotherms indicate that the BET specfic surface area of Co/POMs-6h/NF is about 123.4 m^2 g^{-1} 1.58 times that of Co/NF (78.1 m^2 g^{-1}) and 9.3 times that of POMs/NF (13.2 m^2 g^{-1}) and 21.27 times that of NF(5.8 m^2 g^{-1}), respectively (Fig. S17).

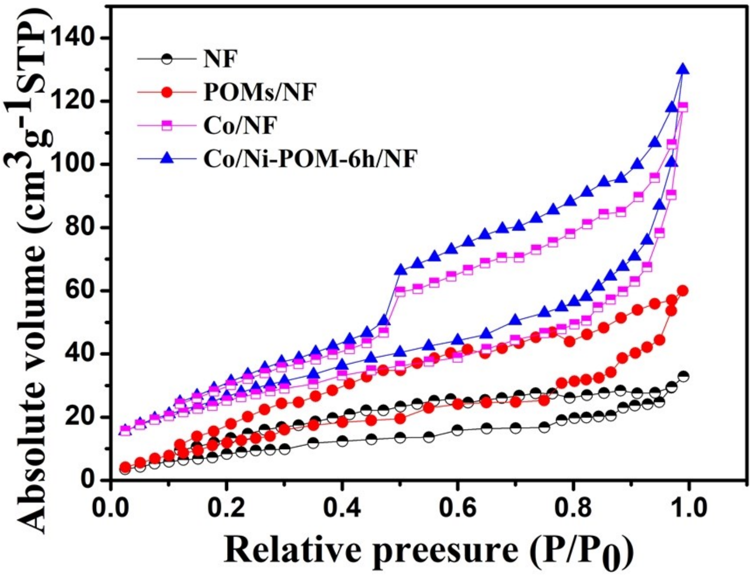

Fig. S17 N_2 sorption isotherms of NF, POMs/NF，Co/NF and Co/Ni-POMs-6h/NF

The morphologies of Co/Ni-POM-6h power can be characterized by SEM, then Fig. S18 present different scales of morphology to gain more details information. The morphology of sample is disorganized, and the entire surface of the Ni foam is also coated Co/Ni-POM through adhesive, which the Co/Ni-POM in form of irregular flower stick structures.

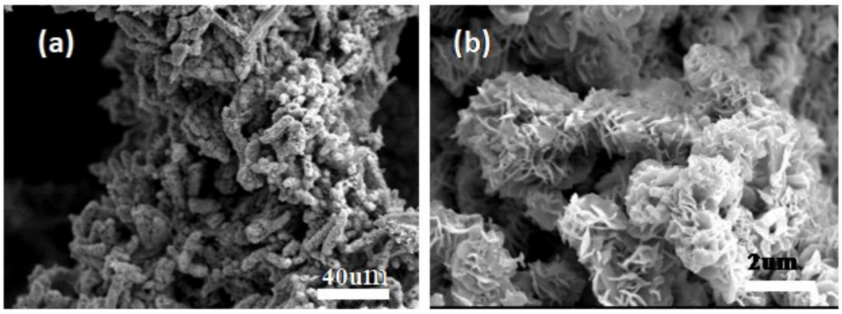

Fig. S18. The different scale SEM images of Co/Ni-POM fixed on Ni foam through adhesive

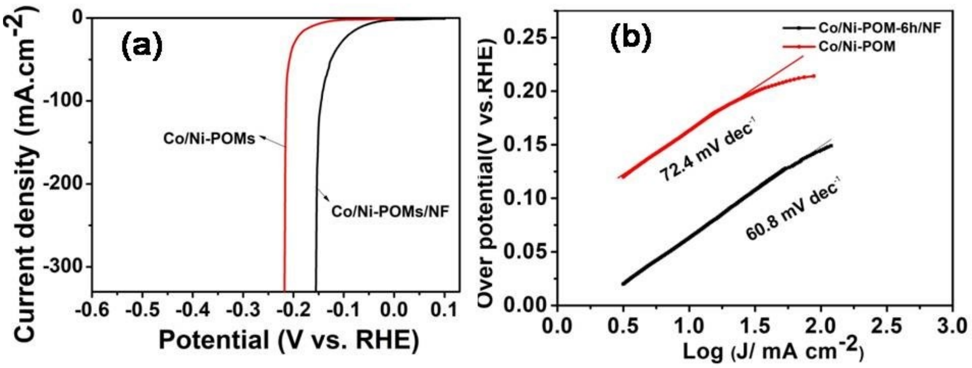

Fig. S19. (a)Polarization curves; (b) Tafel plots for Co/Ni-POM-6h/NF and Co/Ni-POM

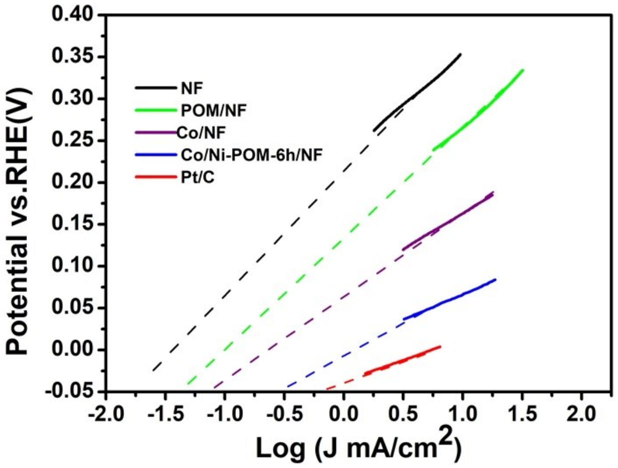

Fig. S20. Calculation of exchange current density of NF, Co/NF, POM/NF, Co/Ni-POM-6h/NF and Pt/C in 1.0 M KOH.

The values of exchange current density (j_0) of Co/NF, POM/NF, Co/Ni-POM-6h/NF are calculated to be 60.2 $\mu A\ cm^{-2}$, 44.6 $\mu A\ cm^{-2}$, and 316 $\mu A\ cm^{-2}$.. The Co/Ni-POM-6h/NF shows the largest exchange current density.

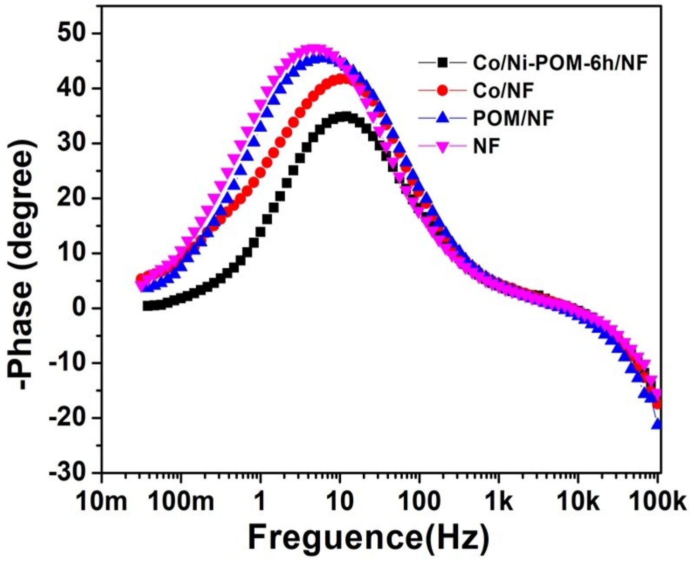

Fig. S21. The Bode plot of NF, Co/NF, POM/NF, Co/Ni-POM-6h/NF at the entire frequency range

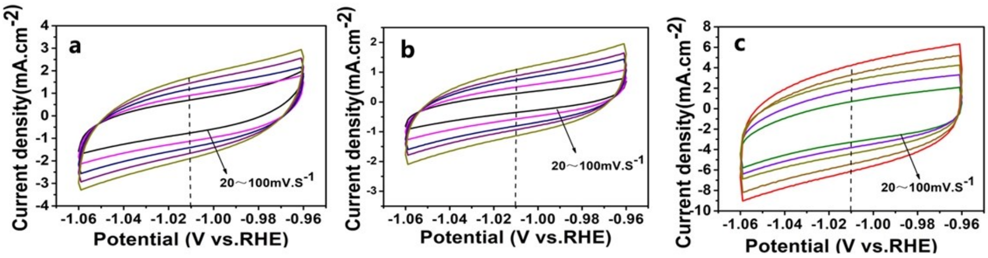

Fig. S22 The CVs of the catalysts recorded from -1.06 to -0.96 V at different rates from 20 to 100 mV s^{-1} for (a) Co/NF; (b) POM/NF; and (c) Co/Ni-POM-6h/NF in 1 M KOH.

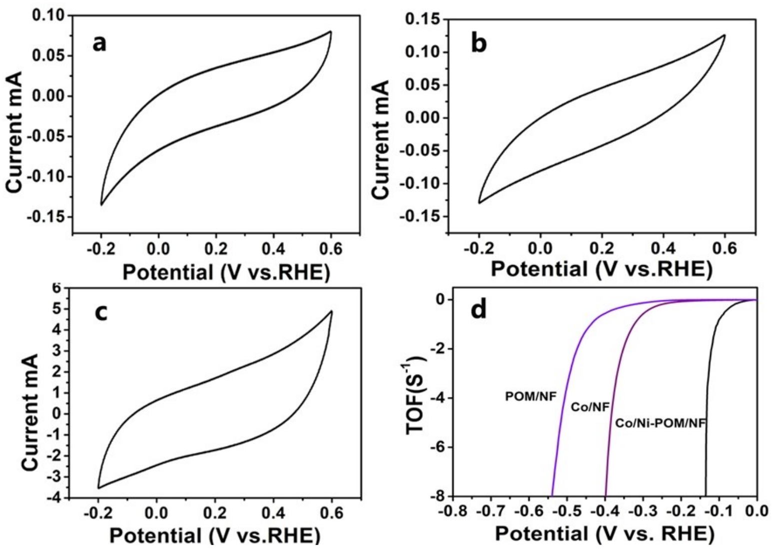

Fig. S23. CVs of (a) Co/NF, (b) POM/NF, and (c) Co/Ni-POM-6h/NF in 1 M PBS (pH = 6.89) with a scan rate of $50mVs^{-1}$. (d) Calculated TOF for Co/NF, POM/NF, Co/Ni-POM-6h/NF in 1 M

KOH.

Table 3. Comparison of HER activity of different POM-based, Ni-based, Ni-modified catalysts.

Catalyst	Reference electrode	Overpotential (mV)	Tafel slope (mV·dec^{-1})	Reference
Ni-S/NF	graphite plate	58	81.6	Materials & Design[1]
Ni3(S0.25Se0.75)2 @NiOOH-8	graphite rod	59	47	Small[2]
Ni$_3$N-VN/NF and Ni$_2$P-VP$_2$/NF	graphite rod	64,147	37, 86	Adv Mater[3]
NiCo$_2$S$_4$/Ni$_3$S$_2$/NF	carbon rod	119	105.2	CS Appl Mater Interfaces[4]
NiM-POM/NF	carbon rod	64	75	Chem. A European[5]
CoP/MoP@NC/CC	graphite rod	98	40,	Applied Catalysis B: Environ.[6]
HWS NiCoP	graphite rod	59	90	Nanoscale[7]
(Co/WN)	graphite rod	48	77	J. MaterChem. A.[8]
NC/Ni$_3$Mo$_3$N/NF	graphite rod	54.6	41.5	Appl. Catal. B Environ.[9]
(Co, Ni)$_2$P/LaF$_3$	Pt foil	94	88	Inorg Chem[10]
(Ni(OH)$_2$/NF)	carbon rod	127	56	ACS Appl Mater Interfaces[11]
Ni$_2$P@NC/NF	graphitic rod	68	64	ACS Sust. Chem. Eng[12]
MoS$_2$/Ni$_3$S$_2$/NF	graphitic rod	76	95	ACS Appl Mater Interface13
NiSe/NF	graphite plate	96	120	Angew Chem Int Ed Engl[14]
Ni2P/Ni/NF	Pt wire	98	72	ACS Cataly.[15]
MoCx@C-1	platinum wire	79	56	J. Mater. Chem. A.[16]
POM@MOF-100	platinum wire	98	45.2	J. Mater. Chem. A.[17]
S-800-1/2	platinum wire	89	45	ACS Appl. Mater. Inter.[18]
HC800	platinum wire	99	83	Chem. Mater[19]
POM@MOFs	platinum wire	180	96	J. Am. Chem. Soc.[20]
POM-based CFs	platinum wire	234	82	J. MaterChem. A.[21]
Co/Ni-POM/NF	carbon rod	68	60.8	This work

Reference:

1 Y. Wu, J. Lian, Y. Wang, J. Sun, Z. He, Z. Gu, , *Mate.Design,* 2021,198 109316.

2 X. Zheng, Y. Zhang, H. Liu, D. Fu, J. Chen, J. Wang, C. Zhong, Y. Deng, X. Han, W. Hu, *Small,* 2018,14,1803666.

3 H. J. Yan, Y. Xie, A. P. Wu, Z. Cai, L. Wang, C. G. Tian, X. M. Zhang, H. G. Fu, , Adv. Mater., 2019,31,901174.

4 H. Liu, X. Ma, Y. Rao, Y. Liu, J. Liu, L. Wang, M. Wu, *ACS Appl. Mater. Interfaces*, 2018,10,10890.

5 X. Jia, C. Streb, Y.F. Song, *Chem. A Euro*. 2019,25,15548.

6Y. J. Tang, H. J. Zhu, L.Z. Dong, A.M. Zhang, S.L. Li, J. Liu, Y.Q. Lan, Applied *CatalyB: Environ*., 2019,245,528.

7] Z. Cai, A. Wu, H. Yan, Y. Xiao, C. Chen, C. Tian, L. Wang, R. Wang, H. Fu, *Nanoscale*, 2018,10,619.

8A. Wu, Y. Gu, B. Yang, H. Wu, H. Yan, Y. Jiao, D. Wang, C. Tian, H. Fu, *J Mater Chem A*, 2020 ,8,22938.

9 Y. K. Chen, J. Y. Yu, J. Jia, F. Liu, Y. W. Zhang, G. W. Xiong, R. T. Zhang, R. Q. Yang, D. H. Sun, H. Liu, W. J. Zhou, *Appl. Catal. B Environ.*, 2020,272,118956.

10 K. Tao, H. Dan, Y. Hai, L. Liu, Y. Gong, *Inorg Chem*, 2020,59,7000.

11 Y. Rao, Y. Wang, H. Ning, P. Li, M. Wu, *ACS Appl Mater Interfaces,*2016, 8,33601.

12 X.W. Lv, Z. P. Hu, L. Chen, J. T. Ren, Y.-P. Liu, Z. Y. Yuan, *ACS Sust. Chem. Eng.,* 2019, 7,12770.

13 J. Cao, J. Zhou, Y. Zhang, Y. Wang, X. Liu, ACS Appl. Mater. Interfaces, 2018, 10,1752,.

14 C. Tang, N. Cheng, Z. Pu, W. Xing, X. Sun, , *Angew Chem. Int Ed. Engl.* 2015,54, 9351,.

15 B. You, N. Jiang, M. Sheng, M.W. Bhushan, Y. Sun, *ACS Cata.l* 2015.6714.

16 X.J. Yang, X.J. Feng, H.Q. Tan, H.Y. Zang, XL. Wang, Y.H. Wang, E.B. Wang, Y.G. Li, *J. Mate. Chem.* A,2016, 4,3947.

17 J. S. Li, Y. J. Tang, C. H. Liu, S. L. Li, R. H. Li, L. Z. Dong, Z. H. Dai, J. C. Bao, Y. Q. Lan, *J. Mater. Chem. A* 2016,4,1202.

18 L. N. Zhang, S. H. Li, H. Q. Tan, S. U. Khan, Y. Y. Ma, H. Y. Zang, Y. H. Wang and Y. G. Li, *ACS Appl. Mater. Inter.*, 2017,9,16270.

19 X. Xu, F. Nosheen, X. Wang, *Chem. Mate.* 2016,28, 6313.

20 J.S. Qin, D.Y. Du, W. Guan, X.J. Bo, Y.F. Li, L.P. Guo, Z.M. Su, Y.Y. Wang, Y.Q. Lan, H.C. Zhou, *J Am. Chem. Soc.* 2015,137,7169.

21 P. P. Zhu, N. Sheng, M. T. Li, J. S. Li, G. D. Liu, X. Y. Yang, J. Q. Sha, M. L. Zhu, J. Jiang, J.Mate. Chem. A,2017, 5,17920.

.